Title	Speckle orientation in paraxial optical systems
Authors(s)	Li, Dayan; Kelly, Damien P.; Kirner, Raoul; Sheridan, John T.
Publication date	2012-02
Publication information	Applied Optics, 51 (4): A1-A10
Publisher	Optical Society of America
Item record/more information	http://hdl.handle.net/10197/3902
Publisher's statement	This paper was published in Applied Optics and is made available as an electronic reprint with the permission of OSA. The paper can be found at the following URL on the OSA website: http://www.opticsinfobase.org/ao/abstract.cfm?URI=ao-51-4-A1. Systematic or multiple reproduction or distribution to multiple locations via electronic or other means is prohibited and is subject to penalties under law.
Publisher's version (DOI)	10.1364/AO.51.0000A1

Speckle orientation in paraxial optical systems

Dayan Li,[1] Damien P. Kelly,[2] Raoul Kirner,[2] and John T. Sheridan[1,*]

[1]Communications and Optoelectronic Research Centre, Science Foundation Ireland—Strategic Research Cluster in Solar Energy Conversion, School of Electrical, Electronic and Communications Engineering, College of Engineering and Architecture, University College Dublin, Belfield, Dublin 4, Ireland

[2]Institut für Mikro- und Nanotechnologien, Macro-Nano, Fachgebiet Optik Design, Technische Universität Ilmenau, Postfach 100565, 98684 Ilmenau, Germany

*Corresponding author: john.sheridan@ucd.ie

Received 3 October 2011; revised 29 November 2011; accepted 30 November 2011; posted 7 December 2011 (Doc. ID 155761); published 25 January 2012

The statistical properties of speckles in paraxial optical systems depend on the system parameters. In particular, the speckle orientation and the lateral dependence (x and y) of the longitudinal speckle size can vary significantly. For example, the off-axis longitudinal correlation length remains equal to the on-axis size for speckles in a Fourier transform system, while it decreases dramatically as the observation position moves off axis in a Fresnel system. In this paper, we review the speckle correlation function in general linear canonical transform (LCT) systems, clearly demonstrating that speckle properties can be controlled by introducing different optical components, i.e., lenses and sections of free space. Using a series of numerical simulations, we examine how the correlation function changes for some typical LCT systems. The integrating effect of the camera pixel and the impact this has on the measured first- and second-order statistics of the speckle intensities is also examined theoretically. A series of experimental results are then presented to confirm several of these predictions. First, the effect the pixel size has on the measured first-order speckle statistics is demonstrated, and second, the orientation of speckles in a Fourier transform system is measured, showing that the speckles lie parallel to the optical axis.

OCIS codes: 030.6140, 030.6600, 110.6150, 070.7345, 050.1940.

1. Introduction

When an optically rough surface is illuminated with coherent light, a three-dimensional (3D) speckle field is generated. The statistical properties of the speckle field are usually examined in an observation plane that is perpendicular to the principal optical axis. Leushacke and Kirchner [1] and Li and Chiang [2] examined the 3D structure of static speckle under plane wave illumination. Later, the 3D space–time cross-correlation function was derived for free-space geometry where a diffuser was illuminated with a Gaussian beam [3]. The analysis in these papers has been extended to include other paraxial optical systems and Gaussian soft apertures by applying the linear canonical transform (LCT) and associated *ABCD* Collins-matrix theory [4,5]. A generalized Yamaguchi correlation factor was also derived for paraxial systems with a hard limiting aperture [6,7]. To analyze fully developed speckle fields [8], the following assumptions are often used to describe the scattered field at the rough surface (the object plane): (i) the autocorrelation of the field at the object plane is a delta function, (ii) the surface is sufficiently optically rough to produce phase variations uniformly distributed over $[0 \rightarrow 2\pi]$, and (iii) the real and the imaginary parts of the field at the rough surface are uncorrelated. With these assumptions speckle fields in the observation plane obey a complex Gaussian random process [8], which mathematically simplifies the derivation of the correlation function.

This correlation function describes the statistical relationship between intensity values at two specific

1559-128X/12/0400A1-10$15.00/0

spatial locations. Unfortunately this also makes it more challenging to directly measure the correlation function with an experiment. In such a speckle experiment, a diffuser of finite size is illuminated with monochromatic laser light, and the intensity values of the speckle field at two different spatial locations are recorded. It is not possible to determine the statistical relationship between these spatial locations with a single measurement. To measure this correlation function, the intensity values at these specific spatial locations should be measured for a large number of different diffusers. We note that, while the diffusers should have similar surface roughness characteristics, it is assumed that each diffuser gives rise to a new statistically independent speckle field. We refer to this averaging as temporal averaging. This type of experiment is time consuming in practice, and so we wish to find another more convenient way to perform this averaging operation. We achieve this using a spatial averaging method, where we can approximately measure the correlation function by allowing recorded intensity values, around the two spatial locations of interest, contribute to the averaging process. In order for this assumption to be strictly valid, it requires that the statistical properties of a speckle field are stationary [9,10], i.e., depend only on the distance between the two spatial coordinates and not on their actual spatial locations. In general paraxial systems, this is not true—the correlation function has a spatial dependency for a Fresnel system [11,12]; however, as we shall see later, it does hold for a Fourier transforming system. Despite this important reservation we have found that the spatial averaging technique works quite well for the experimental systems we have looked at. This implies that the spatial averaging technique is approximately stationary over the region that contributes to the averaging process. For all of the work presented here, we have run a series of numerical simulations where we compare the predictions of temporal and spatial averaging processes for a range of different LCT systems. Good agreement between the two approaches was found when small subimages of speckle intensity are used in the correlation calculation [11,12]. This justifies our interchanging of temporal and spatial averaging for the systems discussed here.

Based on the work in [4], in this paper we explore speckle correlation in general LCT systems. Static speckles in a free-space configuration are orientated radially toward the origin of the optical system [1,3,4], and the longitudinal correlation length is dependent on x and y [11,12]. We note, however, that the speckle orientation and the speckle size (lateral width and longitudinal length) can be varied by introducing a lens into the system [13]. More importantly, in some particular paraxial systems, i.e., a Fourier transform system, the longitudinal length of the speckles become independent of x and y [4]. In this paper we review the theoretical work leading to this conclusion and provide numerical and experimental verification.

When a field is incident on a digital camera, the individual pixels average the light energy incident upon them, in effect filtering and sampling the intensity distribution. This filtering and sampling effect has been analyzed in the context of digital speckle photography [14] and digital holography using *ABCD* formalism [15]. The integrating effect of the finite-size pixel also needs to be considered for a digital speckle pattern. Goodman has pointed out that the first-order statistics of an integrated speckle intensity distribution can be approximated quite well with a gamma function; see Chapter 4 of [8]. The first-order statistics of the background intensity and modulation in phase-shifting speckle interferometry were examined to maximize measurement efficiency [16,17]. Here we extend the derivation of the correlation function following the approach in [8] so that the integrating effect of the camera pixel on the first and second-order speckle statistics in general LCT systems can be examined. This integrating effect can be made negligible provided that the ratio of the camera pixel size to the lateral speckle size is properly controlled. Experimental verification of this result for first-order speckle statistics is presented. The effect of the camera pixel size on the second-order statistical properties of a measured speckle field is also considered. We find that the pixel averaging effect leads to a reduction in the correlation coefficient that would be measured with point detectors, to an extent determined by the ratio of the pixel size to lateral speckle size.

To summarize, the paper is organized in the following manner. In Section 2, we present the results of our theoretical analysis. In Section 3, we compliment these analytical results with a series of robust numerical simulations. In Section 4, we present experimental work that confirms the theory and simulation results from the previous two sections. We then finish with a brief conclusion section.

2. Theoretical Analysis

A. Speckle Properties and Orientations in LCT Systems

In this section we review the derivation of the 3D speckle correlation function. The general LCT optical system where speckles are formed is shown in Fig. 1. A diffuser is placed in the object plane $\boldsymbol{r} = (\xi, \eta)$ and illuminated from behind by a Gaussian beam of wavelength λ. The diameter of the circular beam spot on the diffuser surface is $2w$, where w is the radius at which the beam amplitude drops to $1/e$ of the axial value. The scattered light propagates through an LCT optical system to the observation plane, denoted by $\boldsymbol{\rho} = (x, y)$. According to the Huygens–Fresnel principle [18], the field in the observation plane is given by

$$U(\boldsymbol{\rho}) = \int U_0(\boldsymbol{r}) \exp\left[-\frac{ik}{2B}(Ar^2 - 2\boldsymbol{r}\cdot\boldsymbol{\rho} + D\rho^2)\right] \mathrm{d}^2 r, \tag{1}$$

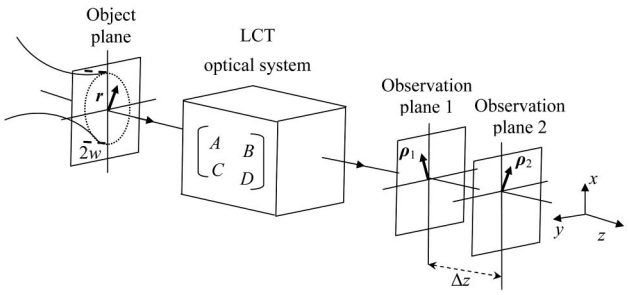

Fig. 1. Static speckle formation that propagates through real-valued *ABCD* optical system. The illuminating spot in the object plane is Gaussian soft aperture with diameter $2w$.

where $U_0(\boldsymbol{r})$ is the scattered field in the object plane and $k = 2\pi/\lambda$, is the wavenumber. The integration is carried out over the entire object plane. A, B, and D are the corresponding Collins-matrix elements, which represent the optical system. In Eq. (2) we list the $\{A, B; C, D\}$ values for some typical operations: Eq. (2a), Fresnel transform (FST), i.e., propagation a distance $z = z_0$ in free space; Eq. (2b), Fourier transform (FT); Eq. (2c), a thin lens with focal length f, i.e., chip modulation transform (CMT). The LCT optical system can be one of these single operations or some combination of them by a simple concatenation of the appropriate matrix, i.e., Eq. (2d) is a single lens system (SLS) where z_1 and z_2 represent the free space before and after a single thin lens of focal length f [5,15,18].

$$\begin{Bmatrix} A & B \\ C & D \end{Bmatrix}_{\mathrm{FST}} = \begin{Bmatrix} 1 & z_0 \\ 0 & 1 \end{Bmatrix}, \tag{2a}$$

$$\begin{Bmatrix} A & B \\ C & D \end{Bmatrix}_{\mathrm{FT}} = \begin{Bmatrix} 0 & f \\ -\frac{1}{f} & 0 \end{Bmatrix}, \tag{2b}$$

$$\begin{Bmatrix} A & B \\ C & D \end{Bmatrix}_{\mathrm{CMT}} = \begin{Bmatrix} 1 & 0 \\ -\frac{1}{f} & 1 \end{Bmatrix}, \tag{2c}$$

$$\begin{Bmatrix} A & B \\ C & D \end{Bmatrix}_{\mathrm{SLS}} = \begin{Bmatrix} 1-\frac{z_2}{f} & z_2 + z_1\left(1-\frac{z_2}{f}\right) \\ -\frac{1}{f} & 1-\frac{z_1}{f} \end{Bmatrix}. \tag{2d}$$

Restricting our attention to fully developed speckle, Goodman's model [8] can be applied to simplify the mathematical derivation. Based on the three assumptions listed in Section 1, the normalized correlation function between the speckle intensities at point positions $\boldsymbol{\rho}_1 = (x_1, y_1)$ in observation plane 1 and $\boldsymbol{\rho}_2 = (x_2, y_2)$ in plane 2 (see Fig. 1) can be given by the ensemble average as [1–5,8]

$$\frac{\langle I(\boldsymbol{\rho}_1) I(\boldsymbol{\rho}_2)\rangle}{\langle I(\boldsymbol{\rho}_1)\rangle \langle I(\boldsymbol{\rho}_2)\rangle} = 1 + C_I(\boldsymbol{\rho}, \Delta\boldsymbol{\rho}, \Delta z), \tag{3}$$

where (following the detailed derivation process in [4])

$$C_I(\boldsymbol{\rho}, \Delta\boldsymbol{\rho}, \Delta z) = \frac{1}{1 + (\Delta z/l_z)^2} \exp\left[-\frac{1}{\rho_0^2} |\Delta\boldsymbol{\rho} - D\Delta z\boldsymbol{\rho}/B|^2\right]. \tag{4}$$

Once again $\boldsymbol{\rho} = (x, y)$, represents one of the observation point positions, and $\Delta\boldsymbol{\rho} = (\Delta x, \Delta y)$ is the lateral coordinate difference between the two observation point positions. When $\Delta z = 0$, the two observation points are in the same observation plane, and C_I is the speckle autocorrelation function. The other parameters appearing in Eq. (4) are defined as follows:

$$l_z = \frac{4B(B + D\Delta z)}{kw^2}, \tag{5a}$$

$$\rho_0 = \frac{2(B + D\Delta z)}{kw} [1 + (\Delta z/l_z)^2]^{1/2}. \tag{5b}$$

The speckle correlation coefficient for a paraxial LCT optical systems for any two points in the 3D space can be determined using Eq. (4). The normalized correlation function $C_I(\boldsymbol{\rho}_1, \Delta\boldsymbol{\rho}, \Delta z)$ has a maximum value of unity, which is obtained when a point in the speckle field is correlated with itself, and the correlation coefficient decreases as the separation between the two correlated points increases. The separation value at which the correlation coefficient falls to the first minimum defines the speckle size [1,2] for this specific direction where separation takes place; thus the speckle shape in the 3D space can be found. For a Gaussian-type correlation function, of the form $\exp(-s^2/\beta^2)$, as examined here, we can define the $1/e$ speckle size to be 2β. Generally, speckles are long narrow cigar-shaped volumes in space [1].

For a given value of Δz, $C_I(\boldsymbol{\rho}_1, \Delta\boldsymbol{\rho}, \Delta z)$ takes its maximum value when $\Delta\boldsymbol{\rho} = \boldsymbol{\rho}\Delta z(D/B)$ (when $B \neq 0$) [4]. This indicates that speckles in different LCT systems have different orientations depending on the choice of B and D. For example, in the free-space propagation case, i.e., FST configuration, $D \neq 0$, so all the speckle grains are orientated radially toward the system origin, while in FT configuration, $D = 0$, and the speckles thus lie parallel to the optical axis [4]. In Fig. 2, we draw some speckle grains in the x–z plane for these two configurations to illustrate this speckle orientation property. We can see the orientation of the speckles have changed to lie parallel to the optical axis immediately after the lens, since for any propagation of the field after the lens, D remains equal to zero; i.e., see Eq. (2d); $D = 0$ when $z_1 = f$. Please note that, for the speckle grains in Fig. 2, only the correlation length in one specific direction is considered, which is denoted by the dashed line. As a result, only the correlation lengths along the dashed lines are comparable for different speckle grains. The lengths are drawn according to the theoretical speckle sizes predicted by the correlation function Eq. (4). In the FST case, the speckles lie orientated along lines that pass

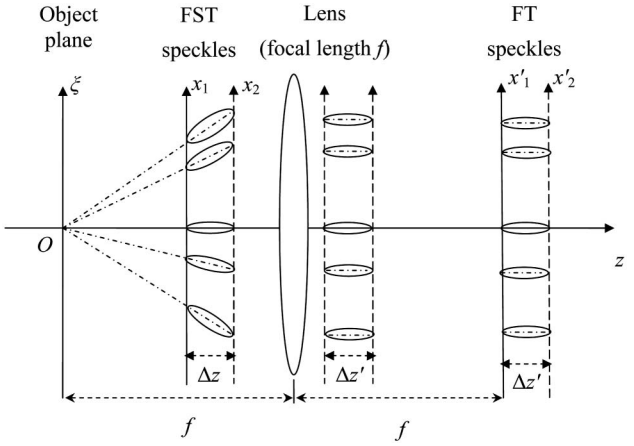

Fig. 2. Schematic demonstration of the orientation of speckle grains (ellipses) in FST configuration and in FT configuration (x–z plane). The dashed lines inside the ellipses denote the correlation lengths of the speckle grain in the corresponding directions. In the right half of this LCT system, the speckle grains all lie parallel to the optical axis and have the same longitudinal correlation lengths.

through the system origin and always have the same projection length onto the optical axis; see [1,10] for detail. As a result, in the directions that pass through the system origin, the further the observation position is away from the optical axis, the larger the speckle grain lengths are. While in the right half of this LCT system (after the lens), the longitudinal speckle correlation is independent of the lateral positions as well as the longitudinal position of the observation plane, which can be inferred using Eq. (4). Thus speckle grains of the same longitudinal length are drawn in the space after the lens. Detailed discussions on the lateral and longitudinal speckle properties in these typical LCT systems will be given in Section 3.

B. First- and Second-Order Statistics of the Integrated Speckle Intensity

In this subsection we explore the role of finite-size camera pixels on the statistical properties of the recorded speckle intensity pattern. For practical measurements, the intensity returned by each camera pixel is in effect the spatially integrated intensity over the finite area of that camera element, and this differs from the ideal pointlike intensity sampling assumed in the standard theoretical derivation. The measured intensity I_α at a single pixel is defined by [8]

$$I_a = \frac{1}{A_D^2}\iint_{-\infty}^{+\infty} D_a(\boldsymbol{\rho}) I(\boldsymbol{\rho}) \mathrm{d}^2\rho, \tag{6}$$

where A_D denotes pixel size, $I(\boldsymbol{\rho})$ is the ideal pointlike speckle intensity incident at the camera detecting surface, and $D_a(\boldsymbol{\rho})$ is the pixel aperture function representing the variation of the camera's photosensitivity over the pixel area.

The second moment of I_α is given by

$$\langle I_{a1} I_{a2}\rangle = \frac{1}{A_D^4}\iint_{-\infty}^{+\infty}\iint_{-\infty}^{+\infty} D_{a1}(\boldsymbol{\rho}_1) D_{a2}(\boldsymbol{\rho}_2) \times \langle I(\boldsymbol{\rho}_1) I(\boldsymbol{\rho}_2)\rangle \mathrm{d}^2\rho_1 \mathrm{d}^2\rho_2, \tag{7}$$

in which the orders of ensemble average and integration have been interchanged. Using Eq. (3) and assuming that $\langle I_a\rangle = \langle I\rangle$, i.e., that the mean of the detected intensity is identical with the true mean of the speckle pattern, Eq. (7) can be rewritten as [8]

$$M^{-1} = \frac{\langle I_{a1} I_{a2}\rangle}{\langle I_{a1}\rangle\langle I_{a2}\rangle} - 1 = \frac{1}{A_D^4}\iint_{-\infty}^{+\infty}\iint_{-\infty}^{+\infty} D_{a1}(\boldsymbol{\rho}_1) D_{a2}(\boldsymbol{\rho}_2) \times C_I(\boldsymbol{\rho}_1, \Delta\boldsymbol{\rho}, \Delta z)\mathrm{d}^2\rho_1 \mathrm{d}^2\rho_2, \tag{8}$$

where we define M^{-1} to be the normalized correlation coefficient for the spatially integrated speckle intensity (second-order statistics) and where $C_I(\boldsymbol{\rho}_1, \Delta\boldsymbol{\rho}, \Delta z)$ is given by Eq. (4). It can be seen from Eq. (8) that M^{-1} is defined by the pixel aperture function $D_a(\boldsymbol{\rho})$ and $C_I(\boldsymbol{\rho}_1, \Delta\boldsymbol{\rho}, \Delta z)$, and M^{-1} is calculated by integrating the corresponding C_I over an area that is limited by D_a. Once the two functions have been found, M^{-1} can be determined for any two pixels.

We begin by examining the simplest case where the speckle intensity at a single pixel in the $z = z_0$ plane is correlated with itself, yielding the autocorrelation coefficient of the integrated speckle intensity. Thus, for Eq. (8) we have $D_{a1}(\boldsymbol{\rho}_1) = D_a(\boldsymbol{\rho}_1)$, $D_{a2}(\boldsymbol{\rho}_2) = D_a(\boldsymbol{\rho}_2)$, and $\Delta z = 0$. The autocorrelation of the integrated speckle intensity is given by

$$M_{\text{auto}}^{-1} = \frac{1}{A_D^4}\iint_{-\infty}^{+\infty} K_D(\Delta\boldsymbol{\rho}) C_I(\boldsymbol{\rho}_1, \Delta\boldsymbol{\rho}, 0)\mathrm{d}^2\Delta\rho, \tag{9}$$

where

$$K_D(\Delta\boldsymbol{\rho}) = \iint_{-\infty}^{+\infty} D_a(\boldsymbol{\rho}_1) D_a(\boldsymbol{\rho}_1 + \Delta\boldsymbol{\rho})\mathrm{d}^2\rho_1. \tag{10}$$

We note from Eq. (4) that $C_I(\boldsymbol{\rho}_1, \Delta\boldsymbol{\rho}, 0)$ in the $z = z_0$ plane is equal to

$$C_I(\boldsymbol{\rho}_1, \Delta\boldsymbol{\rho}, 0) = \exp\left[-\frac{|\Delta\boldsymbol{\rho}|^2}{(2B/kw)^2}\right], \tag{11}$$

which is independent of the position coordinates $\boldsymbol{\rho}_1 = (x_1, y_1)$ but is a function of the coordinate difference $\Delta\boldsymbol{\rho} = (\Delta x, \Delta y)$. Consider a specific case in which the camera pixel aperture function is square in shape and has uniform response (also fill factor = 100%), represented by a rectangle function

$$D_a(x,y) = \begin{cases} 1 & -\frac{A_D}{2} \le x, y \le \frac{A_D}{2} \\ 0, & \text{otherwise} \end{cases}, \tag{12}$$

and identify $A_C = 2[2B/(kw)]$, two times the Gaussian $1/e$ radius in Eq. (11), to be the lateral correlation extent of the speckle pattern incident on the camera; i.e., it quantifies the average lateral speckle size in this specific plane. Substituting Eqs. (11) and (12) into Eq. (9), M_{auto}^{-1} becomes

$$M_{\text{auto}}^{-1} = \frac{A_C^2}{16A_D^4}\exp\left(-\frac{8A_D^2}{A_C^2}\right)\left[A_C - \exp\left(\frac{4A_D^2}{A_C^2}\right)\left[A_C - 2A_D\sqrt{\pi}\,\text{erf}\left(\frac{2A_D}{A_C}\right)\right]\right]^2, \tag{13}$$

where $\text{erf}(x)$ is the standard error function [19].

The autocorrelation coefficient of the integrated speckle intensity M_{auto}^{-1} is a function of the ratio A_D/A_C and is independent of the spatial coordinates where the pixel is located, indicating the integrated intensity at each camera pixel is governed by the same probability density function (PDF). An approximate form of this PDF is the gamma distribution given by (see Subsection 4.6 in [8] and [20])

$$P(I_a) = \frac{1}{\Gamma(M_{\text{auto}})}\left(\frac{M_{\text{auto}}}{\langle I_a\rangle}\right)^{M_{\text{auto}}} I_a^{(M_{\text{auto}}-1)}\exp\left(-\frac{M_{\text{auto}}I_a}{\langle I_a\rangle}\right), \tag{14}$$

where M_{auto} is the inverse of M_{auto}^{-1} and $\Gamma(M_{\text{auto}})$ is a gamma function with argument M_{auto} [19].

Equation (14) describes the first-order intensity statistics of the integrated speckle pattern, which depends on M_{auto}^{-1}. As a result, the form of the PDF depends on the ratio of the camera pixel size, which is normally assumed to be fixed, and the speckle size, which is dependent on the system parameter B. A plot of M_{auto}^{-1} as a function of A_D/A_C is presented in the inset of Fig. 3. We identify three separate regions. The first is (i) the ideal case where we have $A_D/A_C \to 0$, i.e., pointlike detection; M_{auto}^{-1} equals 1. In this region the PDF in Eq. (14) reduces to a negative exponential distribution, which is the standard PDF for fully developed speckle [i.e., see Eq. (14) when $M_{\text{auto}}^{-1} = 1$]. The second is (ii) the extreme case when $A_D/A_C \gg 1$, M_{auto}^{-1} decreases to a very low (close to zero) constant value for a large range of A_D/A_C, indicating that, in this case, the change of the statistics of the speckle intensity, i.e., the correlation extent, A_C, is not detected because the pixel size A_D is too large compared to the average speckle size. The third is (iii) the "Nyquist" range, which lies between $0 \le A_D/A_C \le \pi/8$. This value of $\pi/8$ approximately corresponds to two pixels per speckle [14]. To arrive at this value of $\pi/8$, we follow the same approach as that outlined in Section 2 of [14]; however, our maximum spatial frequency is $4/(\pi A_C)$), not $D/\lambda z$ as in [14], due to the Gaussian nature of the correlation function used here. In practical measurements, we can control and decrease the ratio of A_D/A_C, and as we shall see later on, in our experimental results once $A_D/A_C < \pi/8$, the PDF effectively becomes a negative exponential distribution. As the ratio A_D/A_C exceeds $\pi/8$, combining Eqs. (13) and (14) we see that the PDF of the measured intensity begins to change into a gamma distribution with the argument M_{auto}.

Following the same procedure as that in the derivation of M_{auto}^{-1}, the correlation coefficient of the integrated speckle intensity between two different pixels can be obtained from Eq. (8). Although a closed-form expression for M^{-1} exists (and can be found using a program such as *Mathematica* [21]), we do not present the result here because of its complexity. However in Fig. 3, we plot the calculated value for M^{-1} when one pixel is correlated with other pixels in the same plane. In effect we are plotting the lateral decorrelation function of the integrated speckle. In Fig. 3, we fix $A_C = 2[2B/(kw)]$ and vary A_D to obtain the different A_D/A_C ratios. Again depending on the ratio of A_D/A_C, we see a difference between M^{-1} and C_I, apart from Region (i) identified earlier, i.e., when $A_D/A_C = 0$. As expected, the difference between M^{-1} and C_I reduces as A_D/A_C decreases. From Fig. 3, it appears that the difference between M^{-1} and C_I is more pronounced for smaller values of separation between the two pixels that are being correlated. For example, at the Nyquist rate when $A_D/A_C < \pi/8$, the difference between M^{-1} and C_I

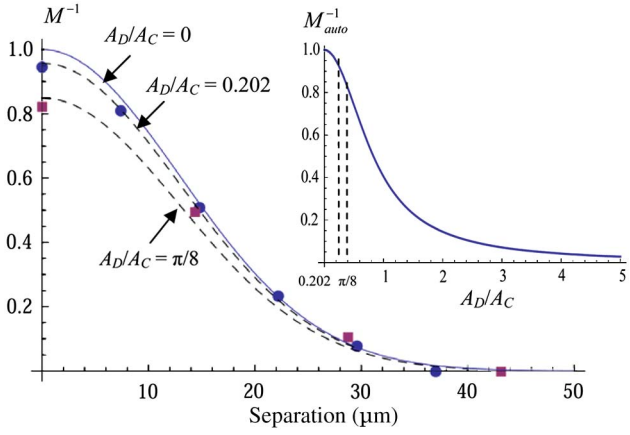

Fig. 3. (Color online) Correlation coefficient of integrated speckle intensity as the ratio of pixel size (A_D) to lateral speckle size (A_C) is varied. Circular and square dots, correlation coefficients calculated when $A_D/A_C = 0.202$ and $A_D/A_C = \pi/8$, respectively; dashed curves: Gaussian fitting of the corresponding dots. Solid curve, correlation coefficient calculated when $A_D/A_C = 0$, which corresponds to the ideal pointlike detection. (Inset) Autocorrelation coefficient of integrated speckle intensity as a function of A_D/A_C.

has a maximum value of 0.17 for the autocorrelation point. From Fig. 3 we see the absolute difference between M^{-1} and C_I; $|M^{-1} - C_I| < 0.17$, once $A_D/A_C \le \pi/8$, i.e., within Region (iii).

3. Numerical Analysis

In this section, simulations of the theoretical correlation function are presented for three typical LCT systems: (I) FST configuration, Fig. 4(a); (II) FT configuration, Fig. 4(b), where $z_1 = z_2 = f$; and (III) SLS, again in Fig. 4(b); however, $z_1 \neq f$. The speckle properties of these different LCT systems are compared.

Before proceeding, we briefly introduce the numerical simulation method used in this paper. For our numerical simulation, the speckle intensities are generated as follows. A square array of dimensions $N \times N$ is used to describe the input field immediately in front of the diffuser, i.e., at the object plane in Fig. 1. Within this square array, Gaussian modulated amplitude values are generated for each array element. A pseudorandom number generator is used to generate uniformly distributed phase values over the interval $[0 - 2\pi]$, which simulates the action of a random phase screen. (Strictly speaking, this violates Goodman's third condition since the real and imaginary parts are not independent; however, it does not appear to change the fundamental statistical properties of the numerically simulated speckle field; see Chapter 2 of [8].) The diameter of the Gaussian amplitude is modeled by a circular shaped subarray containing C samples, which represents the finite extent of the illuminating field on the object surface. This sample number C is defined to be $C = 2w/\Delta\xi$, where $\Delta\xi$ is the sampling period in the object plane. The wave propagation, Eq. (1), is numerically realized using the direct method; see [11,22–24] for details. Speckle intensity images are thus numerically generated in the two observation planes, and the corresponding intensities are found at the points $P_1 = (\rho_1, z_0)$ and $P_2 = (\rho_1 + \Delta\rho, z_0 + \Delta z)$. Running the pseudorandom number generator again, we repeat this process until a large number of intensity values at the same positions P_1 and P_2 are obtained. The two sets of values at P_1 and P_2 make up two vectors, and these are correlated using the built-in Matlab function "normxcorr2" [11,25] to calculate the desired correlation coefficient between the two points.

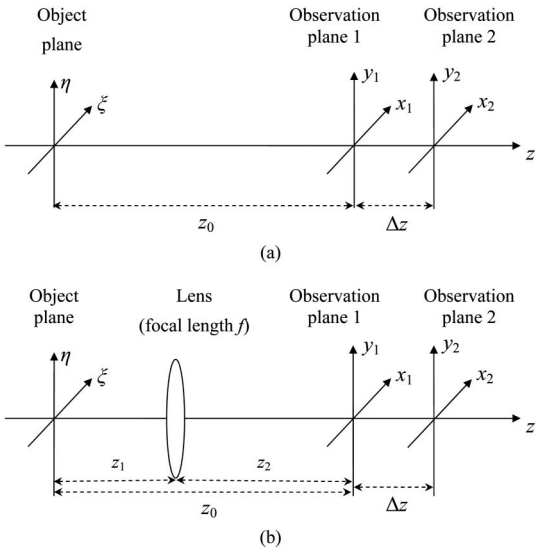

Fig. 4. Schematic representation of (a) an FST configuration, (b) an FT configuration when $z_1 = z_2 = f$, and an SLS, when $z_1 \neq f$.

A. FST Configuration

The simulation results in this configuration have been provided in [11] (see Figs. 3 and 4 in [11]). To save space, we do not repeat them here. A major result is that the speckles in the FST are orientated radially toward the optical system origin [1, 3,4,11,12], as illustrated in Fig. 2, and the longitudinal speckle length decreases dramatically as the observation positions move to off axis.

B. FT Configuration

The schematic representation of the FT configuration is given in Fig. 4(b), with $z_1 = z_2 = f$, and the corresponding $ABCD$ matrix is Eq. 2(b). Because the parameter $D = 0$ after the lens in this configuration, unlike in the FST case, the speckles are orientated parallel to optical axis, and the longitudinal correlation length is independent of the lateral coordinates at the observation positions; see Fig. 2. We provide the theoretical predictions for the speckle correlation coefficients in the x–z plane and the corresponding numerical simulation; see Figs. 5 and 6. Because of the symmetry between the x and y variables in Eq. (4), it is reasonable to set $y = 0$ and $\Delta y = 0$ when examining speckle correlation properties, thus simplifying the analysis. As a result, the theoretical correlation function $C_I(\rho_1, \Delta\rho, \Delta z)$ is examined in the simpler form $C_I(x, 0, \Delta x, 0, \Delta z)$.

The plots in Fig. 5 represent the correlation between speckle fields at $P_1 = (x_1, 0, z_0)$ and $P_2 = (x_1 + \Delta x, 0, z_0 + \Delta z)$ as a function of Δx, and the following parameter values are used: $w = 1.5$ mm, $x_1 = 0.888$ mm, and $B = f = 100$ mm. The maximum lateral correlation value for various Δz all appear at the position where the two observation points

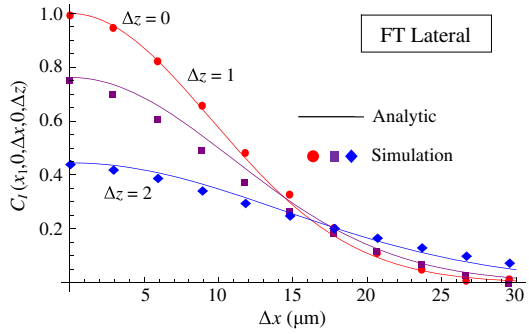

Fig. 5. (Color online) Lateral decorrelation between the off-axis speckles at $P_1 = (x_1, 0, z_0)$ and $P_2 = (x_1 + \Delta x, 0, z_0 + \Delta z)$ in FT configuration. Δz in units of millimeters.

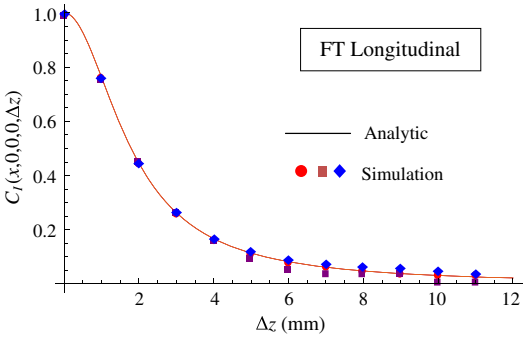

Fig. 6. (Color online) Longitudinal decorrelation of the speckles in the FT configuration. Note that the three plots, for various observation positions $x = 0$ (on-axis), $x = 0.444$ mm, and $x = 0.888$ mm (off-axis), overlap on top of one another.

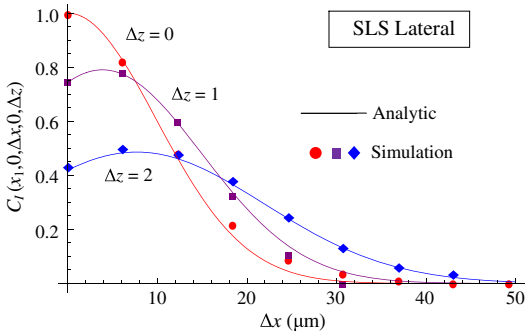

Fig. 7. (Color online) Lateral decorrelation between the off-axis speckles at $P_1 = (x_1, 0, z_0)$ and $P_2 = (x_1 + \Delta x, 0, z_0 + \Delta z)$ in SLS configuration. Δz in units of millimeters.

have no lateral difference (i.e., $\Delta x = 0$), which indicates that the speckles in this system are orientated parallel to the optical axis z. Otherwise, we would observe that the position in Δx of the peak correlation coefficient would change as a function of Δz as in Fig. 7.

Next we examine the longitudinal correlation of the speckles in this configuration, that is the correlation coefficient between the fields at $P_1 = (x, 0, z_0)$ and $P_2 = (x, 0, z_0 + \Delta z)$ as a function of Δz. To study the longitudinal correlation length of the speckles, plots and simulation results for three lateral observation positions, $x = 0$ (on-axis), $x = 0.444$ mm, and $x = 0.888$ mm (off-axis), are provided, as shown in Fig. 6, with $w = 1.5$ mm and $B = f = 100$ mm. The curves for these observations overlap, indicating that the results do not depend on the lateral position, i.e., the value of Δx. As a result, the longitudinal correlation length in the FT configuration does not decrease when the observation position moves off axis, which significantly differs from the corresponding results for the FST [11,12].

C. SLS

The schematic representation of the SLS is presented in Fig. 4(b), where $z_1 \neq f$. The corresponding *ABCD* matrix is Eq. 2(d). In this configuration, similar speckle correlation properties as in the FST case are observed. The speckles in the SLS have nonzero slopes, and the longitudinal correlation length is dependent on the lateral coordinates of the observation positions; see Figs. 7 and 8, respectively.

The plots in Fig. 7 are generated using the following parameter values: $w = 1.5$ mm, $x_1 = 2$ mm, $z_1 = 80$ mm, $z_2 = 120$ mm, and $f = 100$ mm. The maximum lateral correlation values for various Δz all appear at the position where the two observation points (for example, x_1 and x_2) have a particular lateral difference, $\Delta x = x_1 - x_2 = x_1 \Delta z(D/B)$, which indicates that the speckles in the system have slopes $\Delta x/\Delta z$, given by

$$\frac{\Delta x}{\Delta z} = x_1\left(\frac{D}{B}\right). \tag{15}$$

In the FST system, $D = 1$ and $B = z_0$; for a fixed observation point in $z = z_0$ plane, the slope of orientation is fixed. However, in the SLS case, simply by choosing different z_1 and z_2, the speckle orientation for a fixed observation point in $z = z_0$ plane can be controlled.

For the longitudinal correlation of the speckles in this configuration, the correlation coefficient between the fields at $P_1 = (x, 0, z_0)$ and $P_2 = (x, 0, z_0 + \Delta z)$ is obtained. The longitudinal correlation of the speckles for three lateral observation positions $x = 0$ (on-axis), $x = 2$ mm, and $x = 4$ mm (off-axis) are shown in Fig. 8. The other parameter values used are $w = 1.5$ mm, $z_1 = 80$ mm, $z_2 = 120$ mm, and $f = 200$ mm. Figure 8 shows that, similar to the FST case, the longitudinal correlation length in the SLS case decreases as the observation position moves off axis.

Comparing the simulation results presented in the paper to the corresponding analytic predictions, only small differences are observed, indicating the acceptability of the simulations.

4. Experiments

In this section we provide two sets of experimental results. The first set is related to the first-order statistical properties of integrated speckle that are described theoretically in Subsection 2.B. With the second set of experimental results, we demonstrate

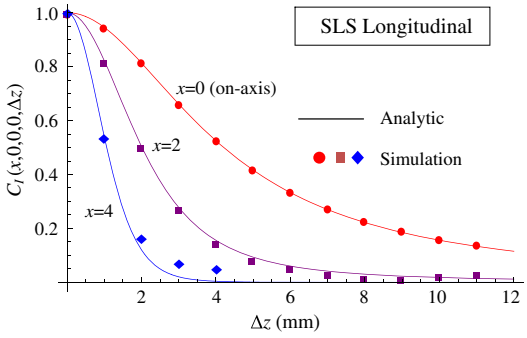

Fig. 8. (Color online) Longitudinal decorrelation of the speckles in the SLS. The three plots, for various observation positions $x = 0$ (on-axis), $x = 2$ mm, and $x = 4$ mm (off-axis), show that speckle longitudinal correlation length depends on the lateral observation position.

that speckles in FT systems are orientated parallel to the optical axis. This latter result in conjunction with [12] demonstrates that the orientation of speckle in paraxial systems can be controlled with a judicious choice of *ABCD* parameters. In both experiments, a spatially filtered and collimated Gaussian beam from a helium–neon laser of wavelength $\lambda = 633$ nm is used as the light source.

A. First-Order Statistics for Integrated Speckle

In this section we first provide experimental results to verify Eq. (14), demonstrating that the first-order statistics of the digitally recorded speckle intensities varies, when the ratio of the pixel size to lateral speckle size changes. The FST configuration is used and schematically represented in Fig. 4(a). Since the theoretical analysis indicates that the effect of the camera pixels should be the same for different LCT systems, this experimental demonstration for the FST case in fact applies more broadly.

Three speckle intensity patterns are captured in planes $z_0 = 80$, 250, and 400 mm. The camera used here was an eight bit four megapxiel *IMPERX* IPX-4M15-G, which has 2048×2048 pixels each of size 7.4 μm. The Gaussian beam diameter was $2w = 8.8$ mm. The intensity values of the central two columns in each image were extracted and used to generate a histogram in order to examine the statistics of the speckle intensities. The height of the histogram is presented in terms of probability density so that it can be compared to the theoretical prediction of Eq. (14), as shown in Fig. 9. In Fig. 9, the blue dashed curves are the theoretical PDFs of the speckle patterns plotted by inserting the appropriate system parameter values into Eq. (14).

From Fig. 9, it can be seen that, for different A_D/A_C ratios, the PDF of the captured intensities varies, and it can be well approximated using the gamma function described in Eq. (14). The integration effect of the pixel transforms the ideal fully developed speckle, for which the PDF follows a negative exponential distribution, into a modified PDF having a gamma distribution. Importantly, as shown in Figs. 9(b) and 9(c), the effect on the experimental results can be minimized by controlling A_D/A_C. In this way, the PDF of the captured speckle intensity reduces to the negative exponential distribution of fully developed speckle and thus made to behave as if it were captured by an ideal pointlike detecting camera. From these experimental results we note that the point at which the PDF can be assumed to be effectively a negative exponential occurs in Fig. 9(b) for a value of $A_D/A_C = 0.323$, which lies within Region (iii), in keeping with the analysis from [14] and the guidelines identified in Subsection 2.B.

We note that, for each of the experimental results presented in Fig. 9, a significant peak appears in the last histogram "bin." We attribute this effect as arising due to a slight saturation of the camera. Thus, there is a slight and artificial increase in the number of pixels over the maximum intensity value, corresponding to a gray level of 255, due to the limited dynamic range of the eight bit camera.

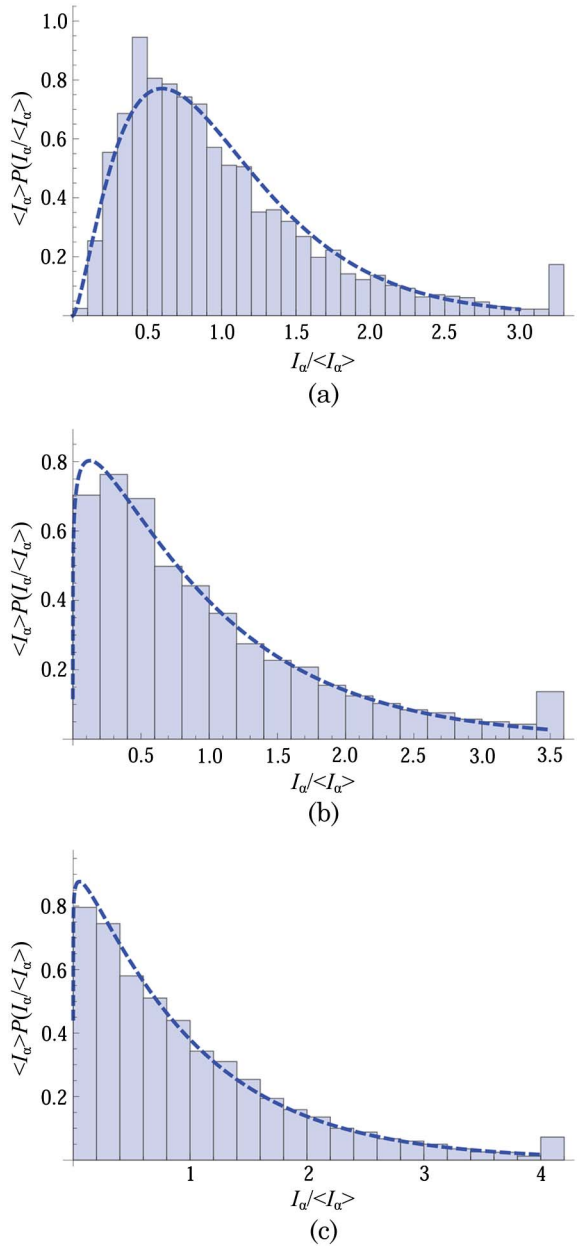

Fig. 9. (Color online) First-order statistics of the captured speckle intensities. The histograms are generated using 4096 intensity values. Dashed blue curves, PDFs of the intensity values predicted using Eq. (14). (a) For speckle pattern captured at $z_0 = 80$ mm; in this case, $A_D/A_C = 1.01$ and $M_{\text{auto}} = 2.4975$. (b) For speckle pattern captured at $z_0 = 250$ mm; in this case, $A_D/A_C = 0.323$ and $M_{\text{auto}} = 1.1420$. (c) For speckle pattern captured at $z_0 = 400$ mm; in this case, $A_D/A_C = 0.202$ and $M_{\text{auto}} = 1.0548$.

B. Speckle Orientation in FT systems

The setup used in this experiment is depicted in Fig. 4(b), with $z_1 = z_2 = f$. An optical diffuser (1500 grit ground glass diffuser) is placed at the object plane, and the spot diameter is set having $2w = 10$ mm. The speckle image is recorded using a CCD camera positioned in the observation plane

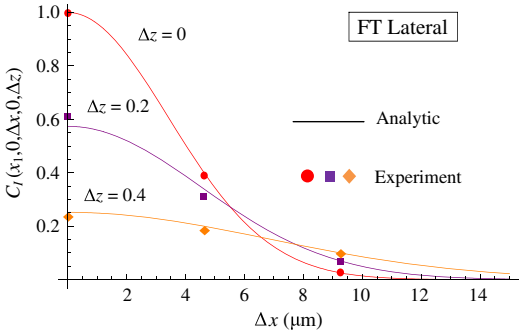

Fig. 10. (Color online) Experimental measurements of the lateral speckle correlation coefficients in FT configuration as a function of lateral displacement Δx of the two correlated speckle fields. Δz in units of millimeters.

that is perpendicular to the optical axis. The CCD is mounted on a manual linear translation stage, having a positional accuracy of ± 20 μm, so that the longitudinal position of the CCD can be controlled. The CCD used for this experiment is an eight bit *KAPPA Dx* 2N, which has 1024×1300 square pixels each of size 4.65 μm.

In the experiment the FT system is produced using a thin lens of focal length $f = 120$ mm. Then 11 speckle patterns are captured over the range of $\Delta z = 1$ mm with step size of 0.1 mm. As in Section 3, we examine the lateral speckle decorrelation by measuring the correlation coefficients between an off-axis point $P_1 = (x_1, 0, z_0)$ and points $P_2 = (x_1 + \Delta x, 0, z_0 + \Delta z)$ as a function of Δx, as shown in Fig. 10. In the figure $x_1 = 2$ mm. The position where the maximum coefficient appears reflects the speckle orientation in this configuration. In the FT system, we see that this maximum coefficient occurs when $\Delta x = 0$. As a result, the orientation of the speckles in the FT system have been made parallel to the optical axis by the thin lens.

For the longitudinal decorrelation, correlation coefficients between a point $P_1 = (x, 0, z_0)$ and points $P_2 = (x, 0, z_0 + \Delta z)$ as a function of Δz are measured, as shown in Fig. 11. Results for on-axis observation

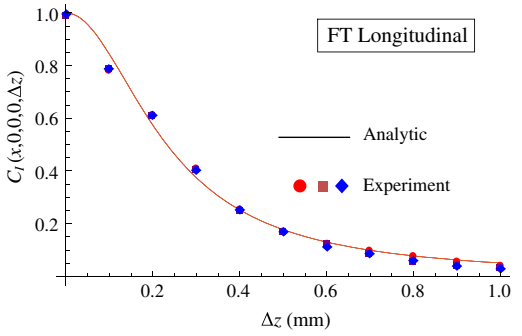

Fig. 11. (Color online) Experimental measurements of the longitudinal correlation coefficients in FT configuration, as a function of longitudinal displacement Δz of the two correlated speckle fields. Note the correlation values for the various observation positions, $x = 0$ (on-axis), $x = 3$ mm, and $x = 6$ mm (off-axis), overlap on top of one another.

point $x = 0$ and off-axis points $x = 3$ mm and $x = 6$ mm in this FT configuration are provided. Here we see that the longitudinal correlation is independent of the lateral position, since the correlation values for the three observation positions overlap with each other.

This latter result may have important applications in speckle metrology. In a $4f$ imaging system, if the speckle size in the Fourier plane is much smaller than the limiting aperture, then we may assume that the Fourier plane speckle field is effectively delta correlated; see [6,26]. In this instance the Fourier plane aperture dominates the speckle properties [26]. If we then consider this Fourier plane aperture to be the input plane of our LCT system, then the speckles in the output image plane will be aligned parallel to the optical axis; see [4,26]. Hence, speckle decorrelation effects should remain approximately invariant over the lateral extent of the image plane unlike the speckles in the image plane of an SLS; see the value of D in Eq. (2d) when $z_1 \neq f$.

5. Conclusions

In this paper we have examined several important and practical issues related to speckle fields in generalized paraxial optical systems. These general optical systems may consist of a sequence of lenses and sections of free space. These optical systems are described with the matrix parameters *ABCD*, and the input and output planes can then be related through an integral relationship known as an LCT. Using this transform, a speckle correlation function that describes the statistical relationship between the intensity values of a speckle field over 3D volume is derived. In our treatment we have assumed that such optical elements are effectively infinite in extent; however, we note that the results presented here can be extended to include Gaussian apertures. Although in this case the *ABCD* parameters can take on complex values, making the correlation function more cumbersome to evaluate. We demonstrated that, by changing the optical elements of the LCT system, the size of the resulting speckles could be controlled. We also specifically examined the orientation of the speckles as a function of these system parameters. Several example systems were discussed and examined in Section 3, with a series of robust numerical simulations, namely (1) Fresnel, (2) Fourier, and (3) single lens systems. For systems (1) and (3), the speckles were shown to have nonzero slope; D is not zero in Eq. 15 in orientation. The angle of orientation the speckles make in a Fresnel system depends on the spatial coordinates ρ and z; however, for (3) the user has more control over this orientation. This arises because the system parameters B and D can be controlled in (3) by varying the lens focal length, f, as well as z_1 and z_2; see Section 3. Because of the nonzero slope, the effective longitudinal speckle size in these systems [(1) and (3)] decreases as the observation point moves away from the optical axis, i.e., as x_1 increases; see Eq. 15. However, in the

case of (2), it was shown that, since the system parameter $D = 0$, the speckles lie parallel to the optical axis, and hence the longitudinal speckle size does not change as a function of x and y. It was shown that the speckle properties in (2) also exist in different LCT domains such as immediately after the lens in Fig. 2. In Section 4 of this paper, we presented experimental results that directly measured the orientation of speckles in a Fourier transforming system, confirming that they lie parallel to the optical axis in keeping with our theoretical predictions, $\Delta x/\Delta z = 0$, since $D = 0$; see Eq. 15.

Another significant topic discussed here was the first- and second-order statistics of integrated speckle fields. This is an important practical consideration since modern detection devices such as CCD cameras average the light energy incident upon them over a finite light-sensitive pixel area. Hence, it is important to understand the difference between the statistical properties of a speckle field in space and those returned by the camera. Following the analysis by Goodman [8], we derived an expression for the first- and second-order statistics of integrated speckle for general LCT systems. By comparing the PDFs for fully developed and integrated speckle, we defined three distinct regions that depend on the ratio of the speckle size A_C and the pixel size A_D. The important practical result from this analysis is that, when $0 \le A_D/A_C \le \pi/8$, we lie within what we term the Nyquist range or Region (iii) as identified in Subsection 2.B. Within this region the first-order PDF of the integrated speckle approximately reduces to a negative exponential distribution, like that for fully developed speckle. Once $A_D/A_C > \pi/8$, the PDF for integrated speckle begins to change into a gamma-type distribution. These first-order theoretical results were demonstrated experimentally in Section 4. Finally we theoretically compared the differences that arise between the second-order statistics for integrated and point detected speckle fields. We have shown to a good approximation that, once one operates within Region (iii), the effects of pixel integration can be neglected.

D. Li is supported by a University College Dublin —China Scholarship Council (UCD-CSC) joint scholarship. We also acknowledge the support of the Science Foundation Ireland (SFI) and Enterprise Ireland under the National Development Plan. D. P. Kelly is a Junior-Stiftungs professor of "Optik Design" and is supported by funding from the Carl-Zeiss-Stiftung.

References

1. L. Leushacke and M. Kirchner, "Three-dimensional correlation coefficient of speckle intensity for rectangular and circular apertures," J. Opt. Soc. Am. A **7**, 827–832 (1990).
2. Q. B. Li and F. P. Chiang, "Three-dimensional dimension of laser speckle," Appl. Opt. **31**, 6287–6291 (1992).
3. T. Yoshimura and S. Iwamoto, "Dynamic properties of three-dimensional speckles," J. Opt. Soc. Am. A **10**, 324–328 (1993).
4. H. T. Yura, S. G. Hanson, R. S. Hansen, and B. Rose, "Three-dimensional speckle dynamics in paraxial optical systems," J. Opt. Soc. Am. A **16**, 1402–1412 (1999).
5. J. E. Ward, D. P. Kelly, and J. T. Sheridan, "Three-dimensional speckle size in generalized optical systems with limiting apertures," J. Opt. Soc. Am. A **26**, 1855–1864 (2009).
6. D. P. Kelly, J. E. Ward, B. M. Hennelly, U. Gopinathan, F. T. O'Neill, and J. T. Sheridan, "Paraxial speckle-based metrology system with an aperture," J. Opt. Soc. Am. A **23**, 2861–2870 (2006).
7. D. P. Kelly, J. E. Ward, U. Gopinathan, B. M. Hennelly, F. T. O'Neill, and J. T. Sheridan, "Generalized Yamaguchi correlation factor for coherent quadratic phase speckle metrology systems with an aperture," Opt. Lett. **31**, 3444–3446 (2006).
8. J. W. Goodman, *Speckle Phenomena in Optics: Theory and Applications*, 1st ed. (Roberts, 2007).
9. X. Zhao and Z. Gao, "Surface roughness measurement using spatial-average analysis of objective speckle pattern in specular direction," Opt. Lasers Eng. **47**, 1307–1316 (2009).
10. D. N. Naik, R. K. Singh, T. Ezawa, Y. Miyamoto, and M. Takeda, "Photon correlation holography," Opt. Express **19**, 1408–1421 (2011).
11. D. Li, D. P. Kelly, and J. T. Sheridan, "Three-dimensional static speckle fields. Part I. Theory and a numerical investigation," J. Opt. Soc. Am. A **28**, 1896–1903 (2011).
12. D. Li, D. P. Kelly, and J. T. Sheridan, "Three-dimensional static speckle fields. Part II. Experimental investigation," J. Opt. Soc. Am. A **28**, 1904–1908 (2011).
13. D. P. Kelly, J. E. Ward, U. Gopinathan, and J. T. Sheridan, "Controlling speckle using lenses and free space," Opt. Lett. **32**, 3394–3396 (2007).
14. M. Sjödahl and L. R. Benckert, "Systematic and random errors in electronic speckle photography," Appl. Opt. **33**, 7461–7471 (1994).
15. D. P. Kelly, J. J. Healy, B. M. Hennelly, and J. T. Sheridan, "Quantifying the 2.5D imaging performance of digital holographic systems," J. Eur. Opt. Soc. Rapid Pub. **6**, 11034 (2011).
16. M. Lehmann, "Phase-shifting speckle interferometry with unresolved speckles: a theoretical investigation," Opt. Commun. **128**, 325–340 (1996).
17. P. K. Rastogi, *Digital Speckle Pattern Interferometry and Related Techniques*, 1st ed. (Wiley, 2001).
18. H. T. Yura and S. G. Hanson, "Optical beam wave propagation through complex optical systems," J. Opt. Soc. Am. A **4**, 1931–1948 (1987).
19. M. Abramowitz and A. Stegun, *Handbook of Mathematical Functions with Formulas, Graphs, and Mathematical Tables*, 9th ed. (Dover, 1972).
20. S. E. Skipetrov, J. Peuser, R. Cerbino, P. Zakharov, B. Weber, and F. Scheffold, "Noise in laser speckle correlation and imaging techniques," Opt. Express **18**, 14519–14534 (2010).
21. Wolfram Research, http://www.wolfram.com/.
22. D. Mas, J. Garcia, C. Ferreira, L. M. Bernardo, and F. Marinho, "Fast algorithms for free-space diffraction patterns calculation," Opt. Commun. **164**, 233–245 (1999).
23. U. Schnars and W. Jueptner, *Digital Holography: Digital Hologram Recording, Numerical Reconstruction, and Related Techniques*, 1st ed. (Springer, 2004).
24. D. P. Kelly, B. M. Hennelly, W. T. Rhodes, and J. T. Sheridan, "Analytical and numerical analysis of linear optical systems," Opt. Eng. **45**, 088201 (2006).
25. Mathworks, http://www.mathworks.com/help/toolbox/images/ref/normxcorr2.html.
26. H. T. Yura, S. G. Hanson, and T. P. Grum, "Speckle: statistics and interferometric decorrelation effects in complex *ABCD* optical systems," J. Opt. Soc. Am. A **10**, 316–323 (1993).